

A novel ultrasound phantom to quantify the effect of slice thickness on imaging performance

Harry Carstairs
Medical Physics
NHS Lothian
Edinburgh, UK
harry.carstairs@ed.ac.uk

Scott Inglis
Medical Physics
NHS Lothian
Edinburgh, UK
scott.inglis@nhslothian.scot.nhs.uk

Stephen D Pye
Medical Physics
NHS Lothian
Edinburgh, UK
stephen.pye@nhslothian.scot.nhs.uk

Carmel M Moran
Centre for Cardiovascular
Science
University of Edinburgh
Edinburgh, UK
Carmel.Moran@ed.ac.uk

Abstract— Whilst it is well understood that linear and linear matrix probes have poorer resolution in the elevation plane than in the scan plane, the impact this has on diagnostic imaging of low contrast anechoic structures is yet to be fully quantified. Previous work [1] has introduced the concept of the resolution integral as a clinically relevant method of quantifying ultrasound imaging performance. This method combines resolution measurements made at different depths to produce a dimensionless figure of merit (R), a characteristic resolution (D_R) and a depth of field (L_R). Over 350 probes have been characterized this way using a standard set of anechoic pipes embedded in an agar based tissue mimicking material (TMM) known as the Edinburgh Pipe Phantom (EPP) [2].

In this study, a modified version of the EPP was constructed using six flat anechoic bars embedded in TMM. The bars were 15 mm wide, assumed to be greater than the slice thickness of three linear (Siemens VF13-5, SonoSite L38x/136 and L38x/10-5) and two multi-row array (Siemens VFX13-5 and VFX9-4) probes. The ability of these probes to image the bars was therefore not dependent on slice thickness. Resolution integrals were measured using this new phantom and compared to results obtained using the EPP.

When slice thickness effects were eliminated, R increased by a factor greater than 2.5 for all probes, and D_R improved by 50-70% compared to values obtained using the EPP. Slice thickness is therefore a significant limiting factor in imaging small anechoic structures using linear and linear matrix probes. This highlights the need for continued use of quality assurance (QA) phantoms such as the EPP that test slice thickness, and for better elevational focusing in clinical applications where the detection of small anechoic structures is a priority.

Keywords— *Edinburgh Pipe Phantom, resolution integral, characteristic resolution, slice thickness*

I. INTRODUCTION

Ultrasound probes typically contain an array of hundreds of individual piezoelectric transducers that are electronically controlled to steer and focus an ultrasound beam [3]. The shape of the ultrasound beam used to generate a B-mode image is therefore a complex function of probe characteristics and user

settings such as number and depth of focal points, making it difficult to formulate a fundamental approach to quantifying the image quality. One approach that has been suggested for making absolute measurements of imaging performance is the resolution integral, first described by Pye and Ellis [1], in which measurements are made of the depth range L over which the lateral resolution is better than a particular value d . In practice, L is measured as the difference between the deepest and most superficial depths at which a pipe presenting a cross-sectional diameter d can be resolved. By interpolating a number of such measurements and calculating the integral $R = \int_0^\infty L d\alpha$, where $\alpha = 1/d$, a dimensionless figure of merit is obtained, a high value of which indicates high resolution over a large depth range [4]. The form and magnitude of this integral also defines (see [2] for details) the characteristic resolution D_R and the depth of field L_R , where $R = L_R/D_R$.

The Edinburgh Pipe Phantom (EPP) contains a series of anechoic pipes of diameters between 0.3 mm and 8 mm embedded at 40° to the vertical in a tank of agar based tissue mimicking material (TMM) [5]. The advantage of using the EPP for resolution integral measurements is the clinical relevance of identifying anechoic structures in tissue (such as vessels and cysts [6,7]), compared to commercial phantoms containing bright nylon filaments or metal targets.

By its geometry, the EPP provides a combined indication of in plane lateral resolution and slice thickness [5]. Whilst slice thickness has long been recognized as an area for improvement in probes [3] and continues to be larger than in plane lateral resolution over the entire depth range of some probes [8], the effect this has on clinical imaging performance is poorly studied.

By modifying the design of the EPP, we show that for linear (1D array) and multi-row array (1.25D) probes, which have limited elevational focusing capabilities, slice thickness severely affects values of R and hence the ability to identify small anechoic structures.

II. METHODS

Recent measurements of standard EPP resolution integrals for five clinical probes were obtained from NHS Lothian and supplemented with additional measurements according to the method described in [5]. The models used were VF13-5, VFX135 and VFX9-4 (Siemens, Erlangen, Germany); and L38x/13-6 and L38x/105 (Sonosite Inc, Bothell, WA, USA). A novel phantom was then designed to eliminate slice thickness whilst otherwise remaining similar to the EPP. Six metal bars of width 15 mm (assumed to be greater than the slice thickness of all tested probes) and thickness of 0.216, 0.263, 0.473, 0.51, 0.57 and 0.98 mm were held diagonally at 39° to the vertical by 3D printed support pieces in a commercially available plastic box with inner dimensions 133×133×160 mm as shown in figure 1.

The tank was filled with a widely used agar TMM [9] with attenuation coefficient of 0.5 dB cm⁻¹ MHz⁻¹ and speed of sound of 1540 ms⁻¹ [10]. Upon setting of the TMM, the support pieces and bars were removed and the voids filled with a mixture of water, glycerol and benzalkonium chloride described in [11].

To take measurements of the depth range L over which each bar was visible, the methodology in [5] was adapted as follows. Probes were aligned vertically with the diagonal of the bars in the image plane, taking care not to apply pressure to the surface of the phantom as this could distort its shape. Scanner settings including transmit and receive frequencies, number and location of focal points, gain, depth range and image enhancement were adjusted before freezing the optimum image of the bottom/top of each bar. A paper slot - of width roughly 15 times the receive ultrasound wavelength as displayed on the screen - was then used to identify the deepest/most superficial part of the bar that was distinguishable from speckle using peripheral vision, and the distance from the top of the slot (for superficial measurements) or the bottom of the slot (for deep measurements) to the top of the image was measured with onscreen calipers. Each measurement was taken as the average of at least three repeats, and the whole process was repeated at least three times for each probe to assess experimental error.

For a bar of thickness t , its cross-section in the lateral plane was taken to be $t/\cos 39^\circ$, giving $\alpha = \cos 39^\circ/t$. This is to be contrasted with the EPP, where the geometric mean of the pipe's cross-section in the lateral and elevation planes is used, giving $\alpha = \sqrt{(\cos 40^\circ/d)}$ for a pipe of diameter d .

A transferable Python module was written to compute R , L_R and D_R from measurements of $L(\alpha)$, according to the definitions given in [2], and is available at https://github.com/harrycrstrs/resolution_integral. This module calculates the most appropriate crossing point of the α axis then interpolates between the data points and numerically integrates to obtain R . A Scipy optimization function was then used to find a straight line between the origin and a point on the $L(\alpha)$ curve that bisects the area under the curve, thereby finding L_R and D_R . The resolution integral module was utilized in the analysis of experimental data, in conjunction with Python libraries Numpy and Pandas.

III. RESULTS

All probes tested were able to resolve the thinnest (0.216 mm) bar of the new phantom (in comparison, none of the probes

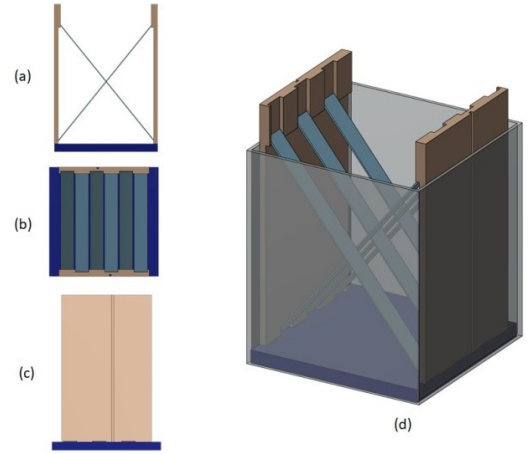


Fig. 1. Design for the bar phantom, modelled using 132D design (Autodesk, California, US). (a) Front view without box. (b) Plan view without box. (c) Side view without box. (d) Three dimensional orthographic view with semi-transparent box. At the bottom is a layer of absorber (purple) to prevent reflections from the base of the plastic box. At either end is a 3D printed support (brown) that holds the bars (blue/grey) in alignment, and has a small gap at the back for ease of removal. The bars are placed on alternate diagonals in order to minimise dead space without introducing a plane of weakness in the TMM.

could image the 0.35 mm diameter pipe of the EPP). However, this made it difficult to estimate where the $L(\alpha)$ curve crossed the α axis, preventing us from reporting precise values of R .

Instead, minimum values for R using the bar phantom (defined as R_{bar}^{min}) were calculated by integrating under $L(\alpha)$ only as far as the last data point. Then, maximum values (defined as R_{bar}^{max}) were calculated by assuming that the resolution could not be smaller than the axial resolution, which was determined for a 'best case' scenario in which the spatial pulse length (SPL) was two wavelengths at the highest transmit frequency v_{max} for each probe, i.e.

$$\text{Axial Resolution} = \text{SPL}/2 = c/v_{max} \quad (1)$$

for a speed of sound $c = 1540\text{ms}^{-1}$. Mathematically, the values we report are

$$R_{bar}^{min} = \int_0^{\alpha^*} \overline{L(\alpha)} d\alpha \quad (2)$$

$$R_{bar}^{max} = \int_0^{c/v_{max}} \overline{L(\alpha)} d\alpha \quad (3)$$

where $\alpha^* = \cos 39^\circ/t$ for the smallest bar of thickness t , and the overline indicates that repeat measurements of L for each bar were averaged before integrating.

Values of v_{max} were 11.43 MHz for the VF13-5 and VFX13-5, 8.89 MHz for the VFX9-4 [12], and estimated to be 10 MHz for the L38x/10-5 and 12 MHz for the L38x/13-6.

Figure 2 plots the range covered by R_{bar}^{min} and R_{bar}^{max} using error bars, and compares this to the results using the EPP for each probe (R_{EPP}). The error bars for R_{EPP} indicate the full range of values obtained by integrating each set of $L(\alpha)$ measurements separately. From this we see that any variability between

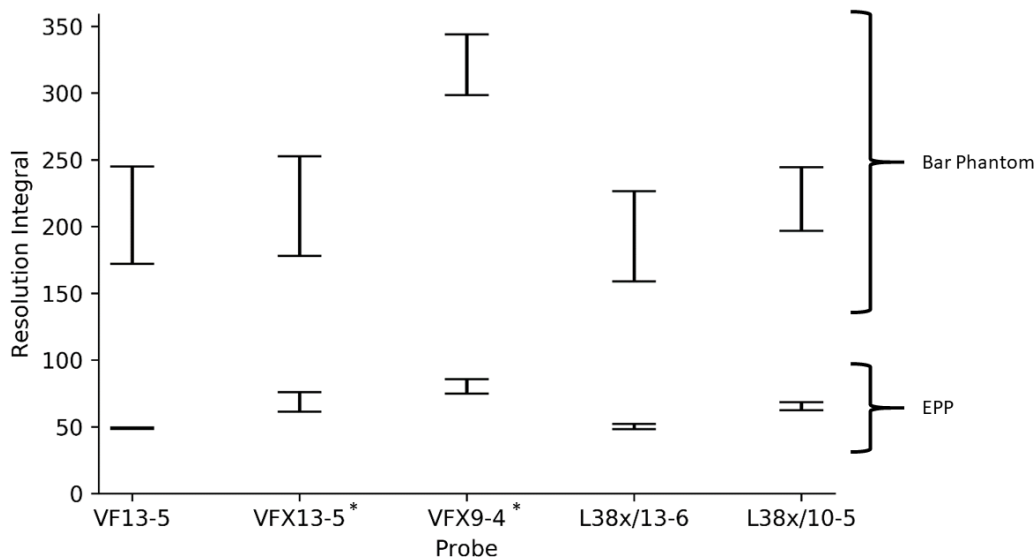


Fig. 2 Resolution integrals measured using the bar phantom and the EPP for 5 linear (*multi-row) probes.

measurements cannot account for the significant increase in R observed with the bar phantom.

For all probes, the minimum values R_{bar}^{min} are greater than R_{EPP} by over 160%, while the maximum values are between 3 and 5 times greater than R_{EPP} . This increase in R was due to a reduction in D_R for every probe, whilst L_R remained unchanged. This is illustrated in figure 3, where the results are plotted on axes of L_R vs D_R , and arrows indicate the change observed upon the removal of slice thickness effects. The mean standard deviation of R measured across all probes and phantoms was 4%.

IV. CONCLUSION

By designing and constructing an ultrasound phantom containing a series of flat bars of varying thicknesses embedded in TMM, the ability of five linear and linear multi-row probes to image anechoic structures based only on their lateral and axial resolutions was quantified. The observed increase in imaging performance was so profound that our phantom could not determine the resolution limit of any of the probes. Nevertheless, it was possible to obtain upper and lower bounds on resolution integral values, showing that R increased by a factor more than 2.6 for all probes, compared to values obtained using the EPP. We conclude from this that slice thickness is a significant limiting factor in imaging small anechoic structures for both linear and linear matrix probes. This highlights the need for awareness of slice thickness among clinical users to mitigate its effects on medical diagnoses; the continued use of QA phantoms such as the EPP that test slice thickness; and improvements in elevational beam focusing to enhance the imaging capabilities of medical probes. The general design of our bar phantom could be improved by increasing its depth and range of bar thicknesses. This would enable higher precision measurements using a wider range of ultrasound probes.

REFERENCES

- [1] S D Pye, W Ellis, and T MacGillivray. "Medical ultrasound: a new metric of performance for grey-scale imaging". *Journal of Physics: Conference Series*, 1:187–192, 2004.
- [2] C M Moran, Scott Inglis, and Stephen D Pye. "The resolution integral – a tool for characterising the performance of diagnostic ultrasound scanners." *Ultrasound*, 22(1):37–43, 2014. PMID: 27433191.
- [3] S.W. Smith, G.E. Trahey, and O.T. von Ramm. "Two dimensional arrays for medical ultrasound." *Ultrasonic Imaging*, 14(3):213 – 233, 1992.
- [4] S D Pye and W Ellis. "The resolution integral as a metric of performance for diagnostic grey-scale imaging." *Journal of Physics: Conference Series*, 279:012009, 2011.
- [5] T. MacGillivray, W Ellis, and S. Pye. "The resolution integral: Visual and computational approaches to characterizing ultrasound images." *Physics in Medicine and Biology*, 55:5067–88, 2010.
- [6] K.T. Wong, Y.Y.P. Lee, A.D. King, and A.T. Ahuja. "Imaging of cystic or cyst-like neck masses." *Clinical Radiology*, 63(6):613 – 622, 2008.
- [7] L. Friedman, K. Finlay, and E. Jurriaans. "Ultrasound of the knee". *Skeletal Radiology*, 30(7):361–377, 2001.
- [8] D. E. Rowland, V. R. Newey, D. P. Turner, and D. K. Nassiri. "The automated assessment of ultrasound scanner lateral and slice thickness resolution: Use of the step response." *Ultrasound in Medicine and Biology*, 35(9):1525 – 1534, 2009.
- [9] Ultrasonics - flow measurement systems - flow test object. International standard, International Electrotechnical Commission, 2001.
- [10] C. Sun, S. D. Pye, J. E. Browne, A. Janeczko, B. Ellis, M. B. Butler et al. "The speed of sound and attenuation of an IEC agar-based tissue-mimicking material for high frequency ultrasound applications." *Ultrasound in Medicine and Biology*, 38(7):1262 – 1270, 2012.
- [11] K. V. Ramnarine, T. Anderson, and P. R. Hoskins. "Construction and geometric stability of physiological flow rate wall-less stenosis phantoms." *Ultrasound in Medicine and Biology*, 27(2):425-250, 2001.
- [12] United Medical Instruments. Siemens Acuson Antares. <https://www.umiultrasound.com/ultrasound-transducers/siemens/acuson-antares>. Accessed 19/03/2019.

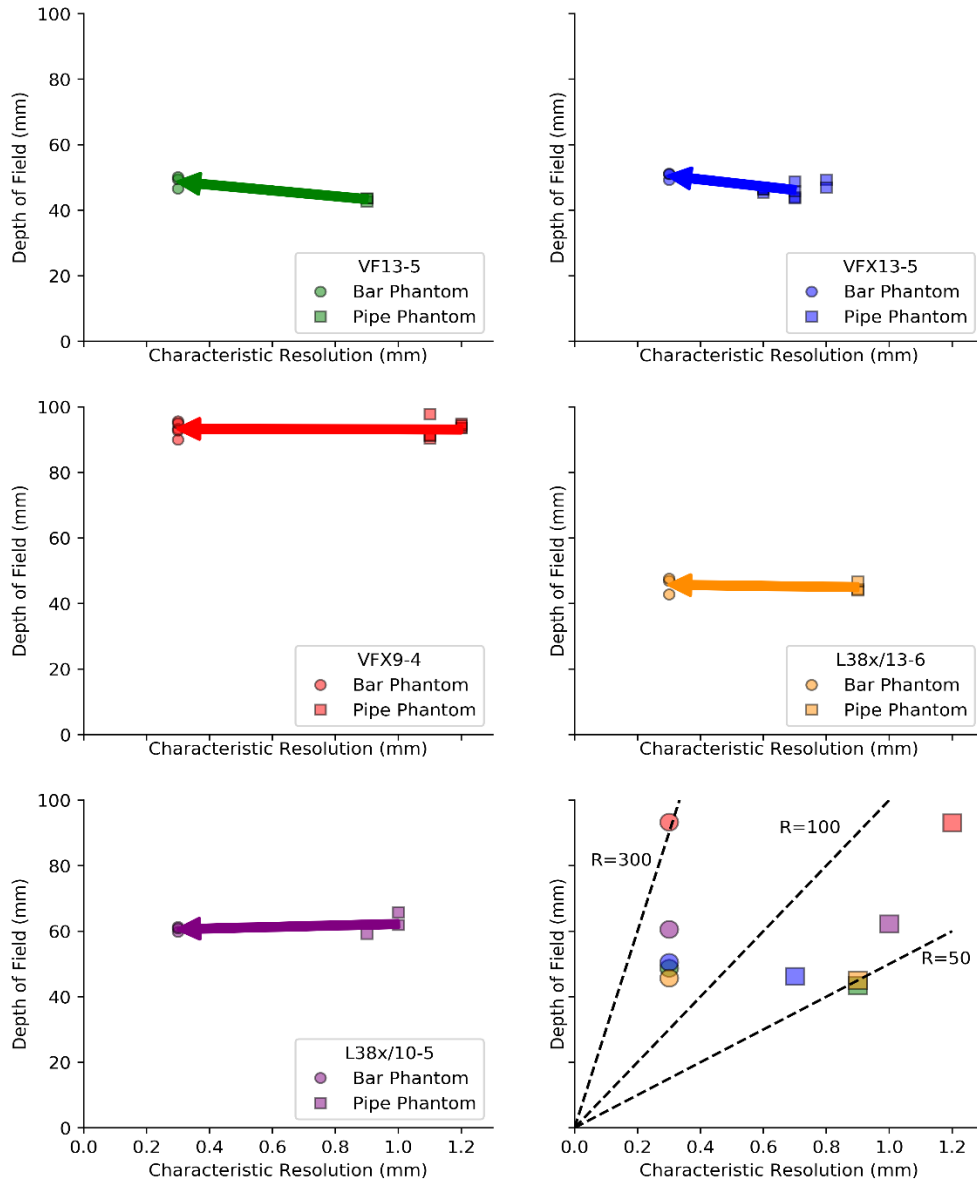


Fig. 3 Comparison of depth of field (L_R) and characteristic resolution (D_R) values obtained for five probes using the EPP (squares) and the new bar phantom (circles). The points represent individual sets of $L(\alpha)$ measurements, while the arrows originate and terminate at the average values for the EPP and bar phantom, respectively. Bar phantom results are the *minimum* values for R and hence *maximum* values of D_R . The bottom right hand plot (where symbols and colours retain their meanings) shows the average results for all probes alongside lines of R equal to 50, 100 and 300.